Synthesis of nanoporous gold by free corrosion of an amorphous precursor

Federico Scaglione, Paola Rizzi, Federica Celegato, Livio Battezzati, " Synthesis of nanoporous gold by free corrosion of an amorphous precursor", Journal of Alloys and Compounds, 615 (2014) S142–S147, http://dx.doi.org/10.1016/j.jallcom.2014.01.239

Synthesis of nanoporous Gold by free corrosion of an amorphous precursor

F. Scaglione[a], P. Rizzi[a], F. Celegato[b], L. Battezzati[a]

[a]Dipartimento di Chimica and NIS, Università di Torino, V. Giuria 7, 10125 Torino, Italy.

[b]INRIM, Strada delle Cacce 91, 10135 Torino, Italy

Abstract

De-alloying of an amorphous precursor is attractive to get a fine microstructure after copious nucleation of crystalline hillocks. However, the noble metal atoms freed on the alloy surface gain high mobility causing coarsening of ligaments. This work describes the de-alloying by free corrosion of a Au-based amorphous alloy in HNO_3 at different temperatures and concentrations. Gold ligaments ranging from 47 to 155 nm have been obtained as a function of acid content. Scanning Electron Microscopy, Transmission Electron Microscopy and X ray Diffraction was used to characterize the nanoporous structure of dealloyed samples. Moreover, an evaluation of the surface diffusion coefficient and of the activation energy and entropy for diffusion of Au adatoms have been performed to study the mechanism of dealloying under free corrosion conditions in comparison with previous studies.

Keywords: A. metallic glasses; C. diffusion; C. corrosion; C. microstructure; D. scanning electron microscopy, SEM; D. X-ray diffraction

1. Introduction

Nanoporous metals are made of a scaffold of interconnected ligaments with pores in between. They can be fabricated by electrochemical or chemical dealloying of either a crystalline phase or an amorphous alloy: the less noble elements are selectively dissolved while the noble components reorganize in ligaments by surface diffusion [1]. The mechanism of de-alloying homogeneous solid solutions such as Ag-Au and Au-Cu, has been recently reviewed with reference to the effect of alloy composition, electrolyte type and temperature on the resultant morphology of ligaments. One established feature is that each grain in the microstructure remains with the original orientation after de-alloying, i. e. it becomes a porous single crystal [1, 2]. A glassy alloy cannot remain amorphous on de-alloying since the removal of elements bring its composition outside the glass forming range, therefore, a crystalline phase rich in the noble component must nucleate and grow. There have been examples of de-alloying amorphous alloys which have shown its feasability in various alloy systems, e. g. Au [3, 4, 5] and Cu based [6, 7, 8, 9], resulting in a ligament/pores microstructure. The occurrence of a randomly oriented polycrystalline phase after de-alloying has also been confirmed [10]. In one case an amorphous alloy, patterned in the supercooled liquid region and then de-alloyed, has shown tunable wettability [11]. The porous structure obtained is of interest for further various applications such as electrocatalysis [12,5], actuators [13], SERS [14], enzyme support [15], for which a key point is represented by the dimension of ligaments and pores formed during dealloying.

Although the need of a nucleation stage in the de-alloying of amorphous alloys has prompted the hope of achieving very fine microstructure, the actual materials turned out to coarsen, a problem already encountered with crystalline alloys [2]. The size of pores and ligaments during coarsening depends on various parameters such as the amount of noble element in the alloy i.e. the parting limit [16, 17], the difference in electrochemical potential between the alloy components, the critical potential for corrosion [18, 19], the composition, pH and temperature of the electrolyte [1]. All these parameters contribute to changing the surface diffusivity of the more noble atoms. Since coarsening can be a problem when reduced dimension of pores and ligaments are required for applications, detailed studies are needed to sort out its causes to control, eventually, the dealloyed microstructure.

In this study, we report on the dealloying of a glassy ribbon of composition $Au_{40}Cu_{28}Ag_7Pd_5Si_{20}$ [20, 21] by free corrosion as a function of temperature and electrolyte concentration with the aim of elucidating aspects of the process when the starting material has amorphous structure and therefore nucleation and growth of crystals must occur to form ligaments. Their coarsening has been studied getting information on the activation surface energy and surface diffusion coefficient of Au adatoms.

2. Experimental

A $Au_{40}Cu_{28}Ag_7Pd_5Si_{20}$ alloy ingot was prepared by arc-melting lumps of pure elements (Au: 99.99%, Ag, Cu and Pd: 99.99%, Si: 99,9995%) in Ti gettered Ar atmosphere. Amorphous ribbons, 2 mm wide and about 25 μm thick, were obtained by melt-spinning the master alloy onto a copper wheel [20, 21].

Samples of 15 mm in length were cut from ribbons. Dealloying by free corrosion was performed as a function of electrolyte concentration in 1, 5, 10 and 14.4 M HNO_3 at 70 °C and as a function of temperature in 10 M HNO_3. Electrolytes have been prepared from chemical grade reagents and deionized water.

Ribbons were analyzed after chemical etching using X-ray diffraction (XRD) in Bragg-Brentano geometry with monochromatic Cu Kα radiation, Scanning Electron Microscopy (SEM), Energy Dispersive X-ray Spectroscopy (EDS) (calibrated with a pure Co sample), High Resolution Transmission Electron Microscopy (HRTEM). Evaluation of scattering domain sizes and lattice parameters was performed by Rietveld analyses of XRD patterns using the MAUD software [22] which incorporates procedures for analysis of the broadening (i. e. the full width at half maximum) and position of Au reflexions.

3. Results

3.1.Effect of the electrolyte concentration

Complete dealloying through the thickness has been obtained for ribbons treated at 70 °C 4 hours in 14.4 M and 10 M HNO_3 and 6 hours in 5 M HNO_3. Ribbons etched 6 hours in 1 M HNO_3 have been partially dealloyed to a thickness of a few microns. Usually the ribbons remain free standing and can be handled for

analyses without damage. Those de-alloyed in the harsher condition, however, at times fractured in the electrolyte producing detached fragments which could be collected and observed in TEM without thinning, thus avoiding the risk of inducing artifacts. SEM images (Fig. 1) provide evidence of formation of a ligament-pore morphology. The porous structure appears to be generally homogeneous and uniform in the whole dealloyed thickness as seen in section-view SEM images (Fig. 1d, 2f and Supporting Information online Fig. S1). EDS analyses have evidenced Si-rich patches placed at random on ligaments (Fig. 1f and 1g). Since enrichment of Si is always accompanied by a high Oxygen signal, it is deduced that Si forms amorphous SiO_2 aggregates. The average ligament size has been measured using a software for image analysis. The results were checked with some manual tests performed with at least one hundred ligaments and resulted to be: 47 ± 12 nm, 79 ± 17 nm, 107 ± 39 nm and 155 ± 37 nm in 1, 5, 10 and 14.4 M HNO_3, respectively. Table 1 summarizes relevant data for these samples.

Diffraction patterns of the as spun ribbon and samples after free corrosion etching are shown in Fig. 3: the intensity of the amorphous halo decreases as a function of concentration while diffraction peaks of an fcc phase occur. According to the Rietveld method, size of scattering domains was evaluated as 14, 22, 19 and 19 nm on increasing the electrolyte concentration while the lattice parameter, a_0, approaches the value of pure Au in 10 and 14.4 M electrolyte (Fig. 4, square symbols).

Apparently, the ligament size is coarser with respect to the size of scattering domains. Fragments of samples dealloyed in 14.4 M HNO_3 were observed in TEM: ligaments appear to be constituted by several crystals as evidenced by the lattice fringes in the HRTEM image reported in Fig. 5 which is representative of the overall shape of ligaments. The zoomed image shows a detail with a few grains. The surfaces of ligaments present rounded contours as shown also by SEM images which are likely due to the sintering of contiguous crystals which were nucleated separately and subsequently impinged on each other during coarsening (see also supporting information online Fig. S2).

3.2. Effect of temperature

Keeping the electrolyte concentration constant, different times of dealloying are needed at a given temperature to provide either fully dealloyed ribbon or at least a portion of ribbon thick enough to be

analyzed without interference from the remaining glassy part. The etching time was 6 hours at 40-90 °C and three days at 20 °C.

XRD patterns of dealloyed samples are analogous to those shown in Fig. 3 (see supplementary information online Fig. S3). The lattice parameter, a_0, after dealloying has been plotted versus temperature in Fig. 4 (triangles). The data suggest that nanoporous Au contains small amount of other elements (e. g. Pd) which were not identified being very likely under the EDS detection limit. Domains resulting from Rietveld analyses have a temperature dependence as 38, 19, 17, 14 nm respectively at 90, 70, 40 and 20 °C.

The ligament-pore morphology is again apparent (Fig. 2) as well as the coarsening of the microstructure. The ligament size has been obtained as 142 ± 43 nm, 92 ± 21 nm, 81 ± 17 nm and 77 ± 17 nm on decreasing the temperature. Patches rich in Si and O have been noticed again on Au ligaments (Fig. 2c). Table 1 summarizes relevant data for these samples.

4. Discussion

4.1. Comparison with electrochemical dealloying

It has been earlier established that the $Au_{40}Cu_{28}Ag_7Pd_5Si_{20}$ amorphous alloy can be electrochemically dealloyed in strong acids by applying a suitable potential. In 1 M HNO_3 at 70 °C rounded nanocrystals of average size of 5 nm were seen in TEM images, oriented in different directions with fine nanopores in between. The ligaments doubled in size after 300 s ending up with size of the order of 130 nm. They were then composed of scattering domains of the order of 60 nm after dealloying for six hours [18].

Under free corrosion the morphology of the ligaments-pores ensemble is similar although figures for both scattering domains and ligaments size are definitely lower in comparable electrolyte concentration. Ligaments are made of several domains here as well. It is inferred that the dealloying mechanism follows the same lines, i.e. nucleation of fcc crystals, their growth to a limited size followed by impingement and coarsening with the continuation of dealloying. The less aggressive environment provided by free corrosion has apparently effect in reducing the mobility of noble metal atoms since the resultant size is smaller. On the other hand, nucleation appears at least as copious since noble metal atoms can form crystal nuclei only once they are freed from the bonding of the other alloy components in the amorphous structure.

The lattice constant of the resultant fcc phase is close, although not identical, to that of Au indicating that a limited amount of other alloy components, most probably Pd, are retained in solid solution.

4.2 Surface Au diffusivity and activation energy for diffusion under free corrosion condition

The mechanism of dealloying involves surface diffusion of adatoms along the surface/electrolyte interface causing growth of crystals and formation of ligaments. This is analogous to the coalescence of particles in de-roughening of Au electrodes [23, 24] in contact with aqueous solutions. The driving force of the process is the decrease in free energy that attends the minimization of particle surface area: the electrode smoothening and coarsening occurs by surface diffusion of adatoms from sites of higher to sites of lower chemical potential.

The equation giving the time dependence of the radius, r(t), of the coarsening particles is $\frac{d(r^4)}{dt} = \frac{2\gamma a_0{}^4 D_s}{kT}$, where k is the Boltzmann constant, T the temperature, γ the surface energy (of the order of 1 Jm^{-2} for Au), a_0 a jump distance taken of the order of the lattice parameter and D_s the surface diffusivity. Integrating the previous equation and using the ligament size d(t) instead of r(t), it was derived $D_s = \frac{d(t)^4 kT}{32\gamma a_0{}^4}$. The values of surface diffusivity were already evaluated for dealloying crystal phases [25, 26, 27]. With amorphous precursors, we have used scattering domains instead of ligament size for d(t) to evaluate surface diffusion coefficients as reported in Table 1. This choice is justified by considering that the mechanism of dealloying fcc solutions and phases having more complex structure differs. Dealloying crystalline alloys provides a network of ligaments in each grain that therefore remains a single crystal and d(t) can be directly determined by high magnification SEM or TEM images [1, 28]. Instead, during dealloying of amorphous precursors, nucleation of a new phase occurs and crystals grow independently by surface diffusion of the more noble element. A model for surface nucleation has not yet been developed, however it was experimentally found that the nucleation frequency is high [18]. During growth, crystals can impinge into each other starting the formation of ligaments. Therefore, while in crystalline alloys the original grains are retained in the nanoporous material, ligaments from an amorphous precursor are constituted by

multiple crystals, as evidenced by HRTEM analysis (Fig. 5 and supporting information online Fig. S2). In this respect it is worth noting that there have been reports on dealloying Al_2Au (fcc, CaF_2 type) and AlAu (monoclinic) [29, 30] as well as Al_2Cu (orthorombic) [31, 32] compounds. The porous fcc Au obtained from Al_2Au retained the original grain structure whereas a nucleation and growth mechanism of either fcc Au or fcc Cu occurred in the case of AlAu and Al_2Cu. The details of these processes are still not fully disclosed, although it appears that an intermediate state can occur in which polycrystalline metal of nanometer size and even amorphous-like zones form before coalescence to conventional ligament-pore microstructure [32]. In depth research on dealloying materials of diverse structures could suggest means for obtaining in a controlled manner such fine microstructures.

Since a change in mechanism for growth is envisaged due to impingement after the first stages of dealloying, the diffusivity is determined from the size of scattering domains which are considered to be more representative of the initial stages of the process. For the present alloy, in 1 M HNO_3 the D_s is one order of magnitude lower under free corrosion ($9.5\cdot10^{-21}$ m^2s^{-1}) than in electrochemical dealloying at 1.05 V ($1\cdot10^{-19}$ m^2s^{-1}). These data are of similar order of magnitude as the few diffusivity values determined during de-roughening of Au reported in literature, though referring to different settings of time, type and temperature of electrolyte (2×10^{-20} m^2s^{-1} in $HClO_4$ 0.1 M at 25 °C [33], 1.2×10^{-18} m^2s^{-1}, in H_2SO_4 0.5 M at 25 °C [34]). The experimental conditions to obtain the lowest D_s values suggest a mean to reduce the coarsening although the dealloying times will inevitably become long.

The activation energy E_a for the surface diffusion process has been evaluated considering the Arrhenius dependence of D_s as a function of temperature, $D_s=D_0exp(-E_a/RT)$, as shown in Fig. 6 with D_0 a pre-exponential factor. E_a results 76 ± 17 kJ mol^{-1}, a value comparable to the literature ones collected in Tab. 2. Specifically, it reproduces the activation energy for surface diffusion derived during dealloying a crystalline $Ag_{65}Au_{35}$ alloy in concentrated HNO_3. Values for Au mobility in other electrolytes appear slightly lower.

The preexponential factor D_0 has been evaluated as $(3)\times10^{-8}$ m^2s^{-1}. The value of entropy of activation for the surface diffusion process, ΔS^*, was deduced from D_0 using the following relation [23]:

$$D_0 = \zeta \frac{b^2 \nu_0}{4} \exp\left(\frac{\Delta S^*}{R}\right)$$

where ζ is the number of contiguous position at which an adatom can jump (equal to 6 for a fcc cubic metal), v_0 the vibrational frequency of the lattice (taken as 10^{12} s^{-1} according to previous reports [23,24]), *b* is the distance between contiguous atoms on the surface (assumed of the order of the interatomic distance in Au, 2×10^{-10} m).

A slightly negative value of ΔS^* has been derived: -6 J $mol^{-1}K^{-1}$. Considering that $\Delta S^* = S_a - S_i < 0$ where S_a is the entropy of the activated state and S_i the entropy of the initial state, than $S_a < S_i$: the activated state S_a is more ordered than the initial state S_i. This is expected since the moving adatom is likely to be placed in a saddle site of the structure which is being reconstructed. In the present case of dealloying an amorphous alloy, the atom in its initial state experiences an environment ordered at short range. Once this is removed by chemical etching, the noble metals will still lack crystalline order. Considering that the activation entropy is reported as +53.4 J $mol^{-1}K^{-1}$ for de-roughening a Au electrode in vacuum [23], one can envisage that the much lower value is due to the interaction of adatoms with ions and molecules in the electrolyte as already supposed for crystalline alloys [24]. The exact nature of these interactions is not yet clear although an effect of different anions has been recently outlined [21]. Inducing specific interactions could allow for better control of the size and morphology of ligaments and pores.

4. Conclusions

The dealloying by free corrosion of $Au_{40}Cu_{28}Ag_7Pd_5Si_{20}$ amorphous ribbon has been performed in HNO_3 solution at different concentration and temperatures leading to a fully nanoporous ribbon in case of concentrated solution and high temperature (70 ˚C – 90 ˚C), while dealloying is slower in diluted solution and closer to room temperature. Morphology and dimension of dealloyed structures made of a fcc phase have been characterized by XRD, Rietveld analysis and SEM images showing the coarsening of pores and ligaments as a function of temperature and electrolyte concentration. The new crystalline phase is almost entirely constituted of Au apart from the one produced at room temperature and 1 M HNO_3 which has a lower lattice constant than that of Au. Silicon is removed in the form of fine patches of amorphous silica.

The XRD data combined with SEM observations suggest that crystal nucleate from the amorphous precursor and grow until impingement with neighboring ones. Further growth completes the formation of ligaments. The ligaments resulted polycrystalline because of the difference in structure between the starting homogeneous phase and the final porous metal.

An analogy is made with experiments of de-roughening Au electrodes for which a model based on surface diffusion is well established. Here the values of the surface diffusivity of Au adatoms in the early stages of the process have been evaluated using the size of scattering domains. The activation energy E_a results close to literature values while the activation entropy is slightly negative suggesting interaction of adatoms with the electrolyte in the activated state also in view of the positive value of entropy reported in the literature [26] for the Au-vacuum interface.

Acknowledgments

This work was supported by "Progetto di Ateneo a valere su Convenzione Intesa SanPaolo, *Advances in nanostructured materials and interfaces for key technologies*". This study has been partly performed at NanoFacility Piemonte, INRIM, a laboratory supported by Compagnia di San Paolo.

Figure Captions

Fig. 1. SEM images of pores and ligaments after free corrosion at 70 °C: a) 6 h in 1 M HNO_3, surface-view, b) 6 h in 5 M HNO_3, surface-view, c) 6 h in 5 M HNO_3, section-view, d) enlargement of c), e) 4 h in 10 M HNO_3, surface-view; f) 4 h in 14.4 M HNO_3, surface-view; g) EDS analyses of patches on ligaments.

Fig. 2. SEM images of pores and ligaments after free corrosion in 10 M HNO_3 at: a) 20 °C, surface-view; b) 40 °C, surface-view; c) 70 °C, surface-view; d) 90 °C, surface-view; e) 40°C, section-view, f) enlargement of e). On ligaments of figure c) circles highlight SiO_2 patches.

Fig. 3. XRD patterns given by the as-spun ribbon (a) and samples de-alloyed at 70 °C for 6 hours in 1 and 5 M (b, c) and 4 hours in 10 and 14.4 M HNO_3 (d, e).

Fig. 4. Lattice parameter a_0 obtained from Rietveld analyses as a function of temperature (triangles) and electrolyte concentration (square symbols).

Fig 5: HRTEM image of a sample dealloyed at 70°C in 14.4 M HNO_3 providing a general view of a ligament. The zoomed image shows details of some grains and their boundaries.

Fig. 6 Plot of $\ln D_s$ vs. T^{-1} for the estimation of the activation energy.

Table 1. Scattering domains of nanoporous gold obtained by free corrosion at different T and [M] and corresponding surface diffusivity of Au adatoms.

Table 2. Values of E_a, D_0 and ΔS^* from the literature. Negative values spanning a wide range refer to de-roughening experiments performed at increasing potential. Data in brackets were computed in this work from values given in the respective reference.

References

[1] J. Erlebacher, R. Seshadri, Hard Materials with Tunable Porosity, MRS Bull. 34 (2009) 561–568.
[2] J.Weissmuller, R.C.Newman, H.Jin, A.M.Hodge,, J.W.Kysar, Nanoporous metals by alloy corrosion: formation and mechanical properties, MRS Bull. 34 (2009) 577
[3] F. Scaglione, A. Gebert, L. Battezzati, Dealloying of an Au-based amorphous alloy, Intermetallics 18 (2010) 2338-2342.
[4] L. Battezzati, F. Scaglione, De-alloying of rapidly solidified amorphous and crystalline alloys, Journal of Alloys and Compounds 509S (2011) S8–S12.
[5] C. Chen, S. Zhu, X. Yang, L. Pi, Z. Cui, Electro-oxidation of ethylene glycol on nanoporous Ti-Cu amorphous alloy, Electrochimica Acta 56 (2011) 10253-10258.
[6] Z. Dan, F. Qin, Y. Surgawara, I. Muto, N. Hara, Fabrication of ultrafine nanoporous copper by the minor addition of gold, Mater. Trans, 10 (2012) 1765-1769.
[7] H. Abe, K. Sato, H. Nishikawa, T. Takemoto, M. Fukuhara, A. Inoue, Dealloying of Cu-Zr-Ti bulk metallic glass in hydrofluoridic acid solution, Mater Trans, 6 (2009) 1255 – 1258.
[8] T. Aburada, J.M. Fitz-Gerald, J.R. Scully, Synthesis of nanoporous copper by dealloying of Al-Cu-Mg amorphous alloys in acidic solution: the effect of nickel, Corr. Sci, 53 (2011) 1627-1632.
[9] Z. Dan, F. Qin, Y. Surgawara, I. Muto, N. Hara, Fabrication of nanoporous copper by dealloying amorphous binary Ti-Cu alloys in hydrofluoric acid solutions, Intermetallics 29 (2012) 14-20.
[10] J. Yu, Y. Ding, C. Xu, A. Inoue, T. Sakurai, M. Chen, Nanoporous metals by dealloying multicomponent metallic glasses, Chem. Mater. 20 (2008) 4548-4550.
[11] H.S. Arora, Q. Xu, Z. Xia, Y. Ho, N.B. Dahotre, J. Schroers, S. Mukherjee, Wettability of nanotextured metallic glass surfaces, Scripta Mat. 69 (2013) 732–735.
[12] X.Y. Lang, H. Guo, L.Y. Chen, A. Kudo, J.S. Yu, W. Zhang, A. Inoue, M.W. Chen, Novel Nanoporous Au-Pd Alloy with High Catalytic Activity and Excellent Electrochemical Stability, J. Phys. Chem. C 114 (2010) 2600–2603.
[13] H.J. Jin, J. Weissmüller, Bulk Nanoporous Metal for Actuation, Adv. Eng. Mater. 12 (2010), 714–723.
[14] G. Li, X. Song, Z. Sun, S. Yang, B. Ding, S. Yang, Z. Yang, F. Wang, Nanoporous Ag prepared from the melt-spun Cu-Ag alloys, Solid State Sci. 13 (2011) 1379–1384.
[15] M. Hakamada, M. Takahashi, M. Mabuchi, Enhanced thermal stability of laccase immobilized on monolayer-modified nanoporous Au, Mater. Letters, 66(2012) 4-6.
[16] K. Sieradzki, N. Dimitrov, et al., The Dealloying Critical Potential, J. Electrochem. Soc. 149 (2002) B370–B377.
[17] D.M. Artymowicz, J. Erlebacher, R.C. Newman, Relationship between the parting limit for de-alloying and a particular geometric high-density site percolation threshold, Phil. Mag.89 (2009) 1663–1693.
[18] H.W. Pickering, P.J. Byrne, On Preferential Anodic Dissolution of Alloys in the Low-Current Region and the Nature of the Critical Potential, J. Electrochem. Soc. 118 (1971) 209–215.
[19] H.W. Pickering, Characteristic Features of Alloy Polarization Curves, Corros. Sci. 23 (1983) 1107–1120.
[20] F. Scaglione, P. Rizzi, L. Battezzati, De-alloying kinetics of an Au-based amorphous alloys, J. Alloys Comp. 536 (2012) S60–S64.
[21] P. Rizzi, F. Scaglione, L. Battezzati, Nanoporous gold by dealloying of an amorphous precursor, J. Alloys Comp. (2012), http://dx.doi.org/10.1016/j.jallcom.2012.11.029.
[22] S.M. L. Lutterotti, H.-R. Wenk,, MAUD (Material Analysis Using Diffraction) is released under free license of the authors. Available at: http://www.ing.unitn.it/wmaud/index.html.

[23] J.M. Dona, J. Gonzalez-Velasco, Mechanism of Surface Diffusion of Gold Adatoms in Contact with an Electrolytic Solution, J. Phys. Chem. 97 (1993) 4714–4719.
[24] C. Alonso, R.C. Salvarezza, J.M. Vara and A.J. Arvia, The surface diffusion of gold atoms on gold electrodes in acid solution and its dependence on the presence of foreign adsorbates, Electrochem. Acta, 9 (1990) 1331–1336.
[25] Z. Zhang, Y. Wang, Y. Wang, X. Wang, Z. Qi, H. Ji, C. Zhao, Formation of ultrafine nanoporous gold related to surface diffusion of gold adatoms during dealloying of Al2Au in an alkaline solution, Scripta Mater. 62 (2010) 137–140.
[26] L.H. Qian, M.W. Chen, Ultrafine nanoporous gold by low-temperature dealloying and kinetics of nanopore formation, Appl. Phys. Lett. 91 (2007) 083105.
[27] G. Andreasen, M. Nazzarro, J. Ramirez, R.C. Salvarezza, A.J. Arvia, Kinetic of Particle Coarsening at Gold Electrode/Electrolyte Solution Interfaces Followed by in Situ Scanning Tunneling Microscopy, J.Electrochem. Soc. 143 (1996) 466–471.
[28] S.V. Petegem, S. Brandstetter, R. Maass, A.M. Hodge, B.S. El-Dasher, J.r. Biener, B. Schmitt, C. Borca, H.V. Swygenhoven, On the Microstructure of Nanoporous Gold: An X-ray Diffraction Study, Nano Lett. 9 (2009) 1158–1163.
[29] Q. Zhang, X. Wang, Z. Qi, Y. Wang, Z. Zhang, A benign route to fabricate nanoporous gold through electrochemical dealloying of Al–Au alloys in a neutral solution, Electrochim. Acta 54 (2009) 6190-6198
[30] Z. Zhang, Y. Wang, Z. Qi, C. Somsen, X. Wang, C. Zhao, Fabrication and characterization of nanoporous gold composites through chemical dealloying of two phase Al-Au alloys, J. Mater. Chem., 19 (2009) 6042-6050
[31] W.B. Liu, S.C. Zhang, N. Li, J.W. Zheng, Y. L. Xing, Influence of phase constituent and proportion in initial Al–Cu alloys on formation of monolithic nanoporous copper through chemical dealloying in an alkaline solution, Corros. Sci., 53 (2011) 809
[32] W.B. Liu, S.C. Zhang, N. Li, J.W. Zheng, S.S. An, Y. L. Xing, Dealloying Behavior of Dual-Phase Al 15 at.% Cu Alloy in an Acidic Solution, Int. J. Electrochem. Sci., 7 (2012) 2240-2253
[33] A. Dursun, D.V. Pugh, S.G. Corcoran, Dealloying of Ag-Au alloys in Halide-Containing Electrolytes Affected on Critical Potential and Pore SizeJ. Electrochem. Soc. 150 (2003) B355-B360.
[34] M.P. García, M.M. Gómez, R.C. Salvarezza, A.J. Arvia, Effect of the solution composition and the applied potential on the kinetics of roughness relaxation at gold electrodes in slightly acid electrolytes, J. Electroanal. Chem. 347 (1993) 237–246.
[35] C. Alonso, R.C. Salvarezza, J.M. Vara, A.J. Arvia, L. Vazquez, A. Bartolome and A.M. Baro, The Evolution of Surface Diffusion Coefficients of Gold and Platinum Atoms at Electrochemical Interfaces from Combined STM-SEM Imaging and Electrochemical Techniques, J. Electrochem. Soc, 137 (1990) 2161–2166.

Table

Conc. [M]	Temp. [°C]	Scat. domains [nm]	D_s $[m^2s^-]^1$	Conc. [M]	Temp. [°C]	Scat. domains [nm]	D_s $[m^2s^-]^1$
1	70	14	9.5×10^{-21}	10	20	14	6×10^{-22}
5	70	22	5.5×10^{-20}	10	40	17	1.8×10^{-20}
10	70	19	3.4×10^{-20}	10	70	19	3.4×10^{-20}
14.4	70	19	4.8×10^{-20}	10	90	38	5.2×10^{-19}

Table

Reference	Sample	Electrolyte	E_a kJ mol^{-1}	D_0 m^2s^{-1}	ΔS* $Jmol^{-1}K^{-1}$
[25] Z. Zhang	Al_2Au	20 wt.% NaOH	60.1±2.9	6.2×10^{-11}	[-57.2]
[23] J.M. Dona	Au	0.5 H_2SO_4	55.1-14.3	1.6×10^{-9}-1.3×10^{-17}	-30.9 -184.9
[35] C. Alonso	Au	0.5 H_2SO_4	59	-	-
[35] C. Alonso	Pt	0.5 H_2SO_4	79	-	-
[26] L.H. Qian	$Ag_{65}Au_{35}$	70% HNO_3	74±3	[3.4×10^{-6}]	[33.5]

Figure

Click here to download high resolution image

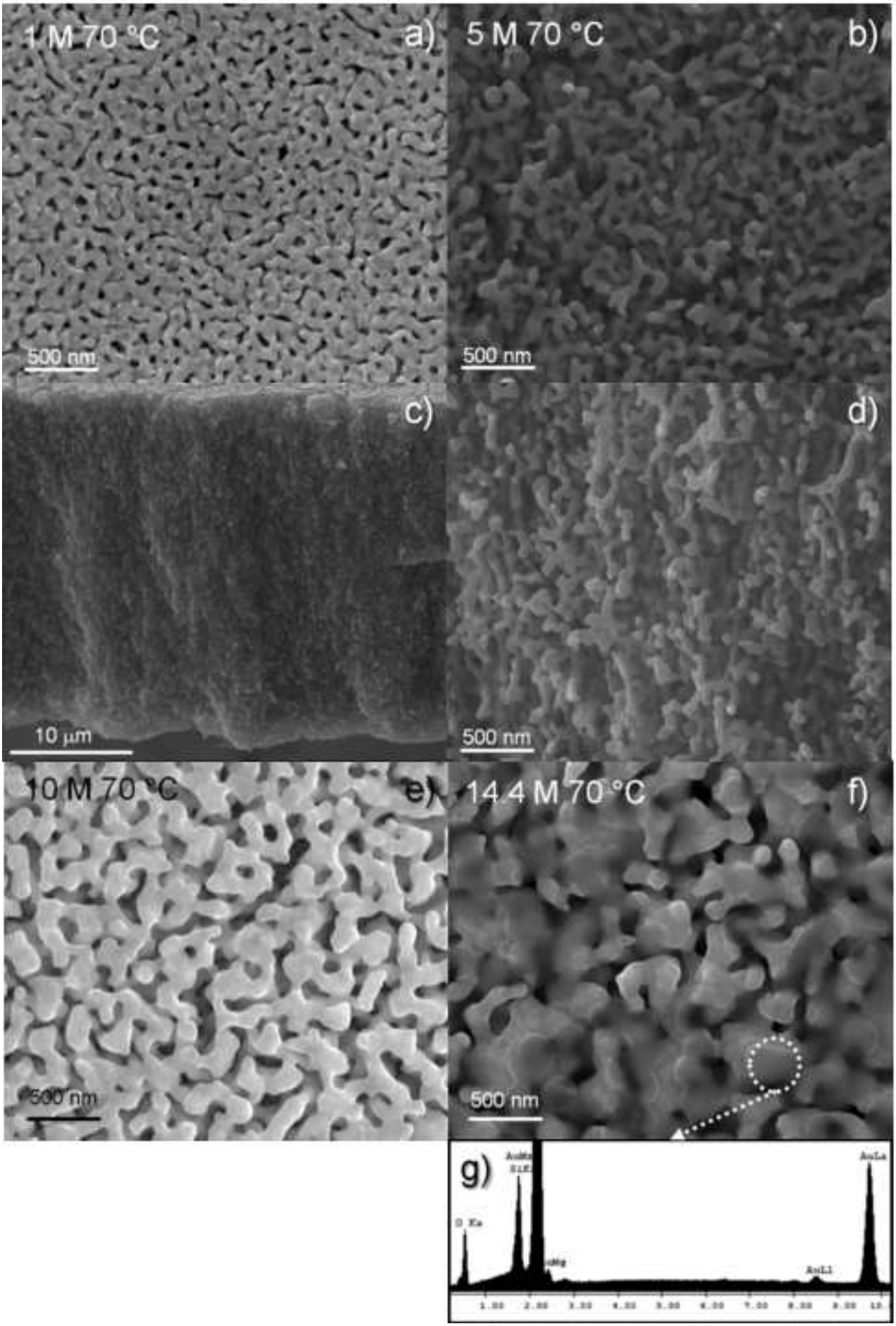

Figure
Click here to download high resolution image

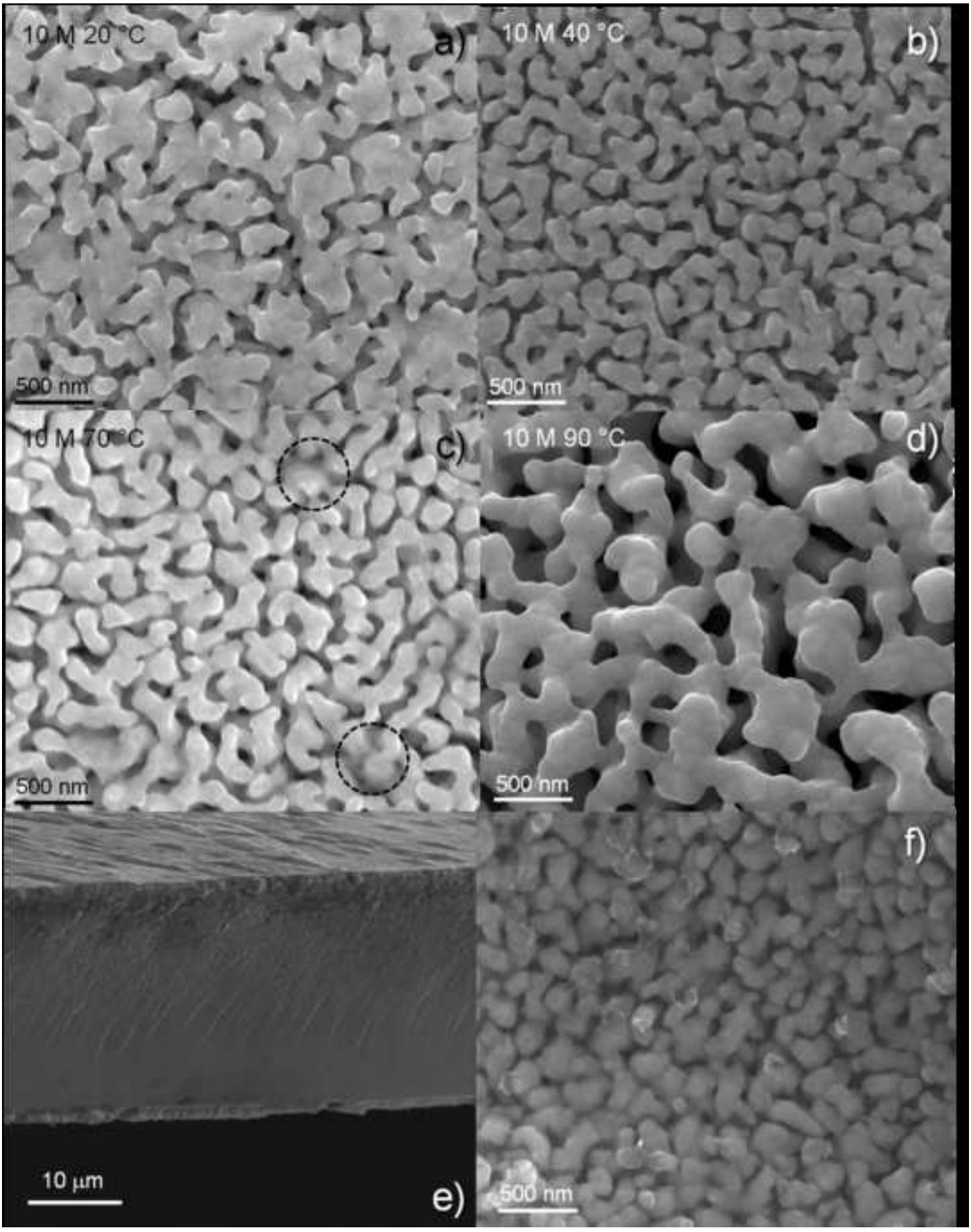

Figure

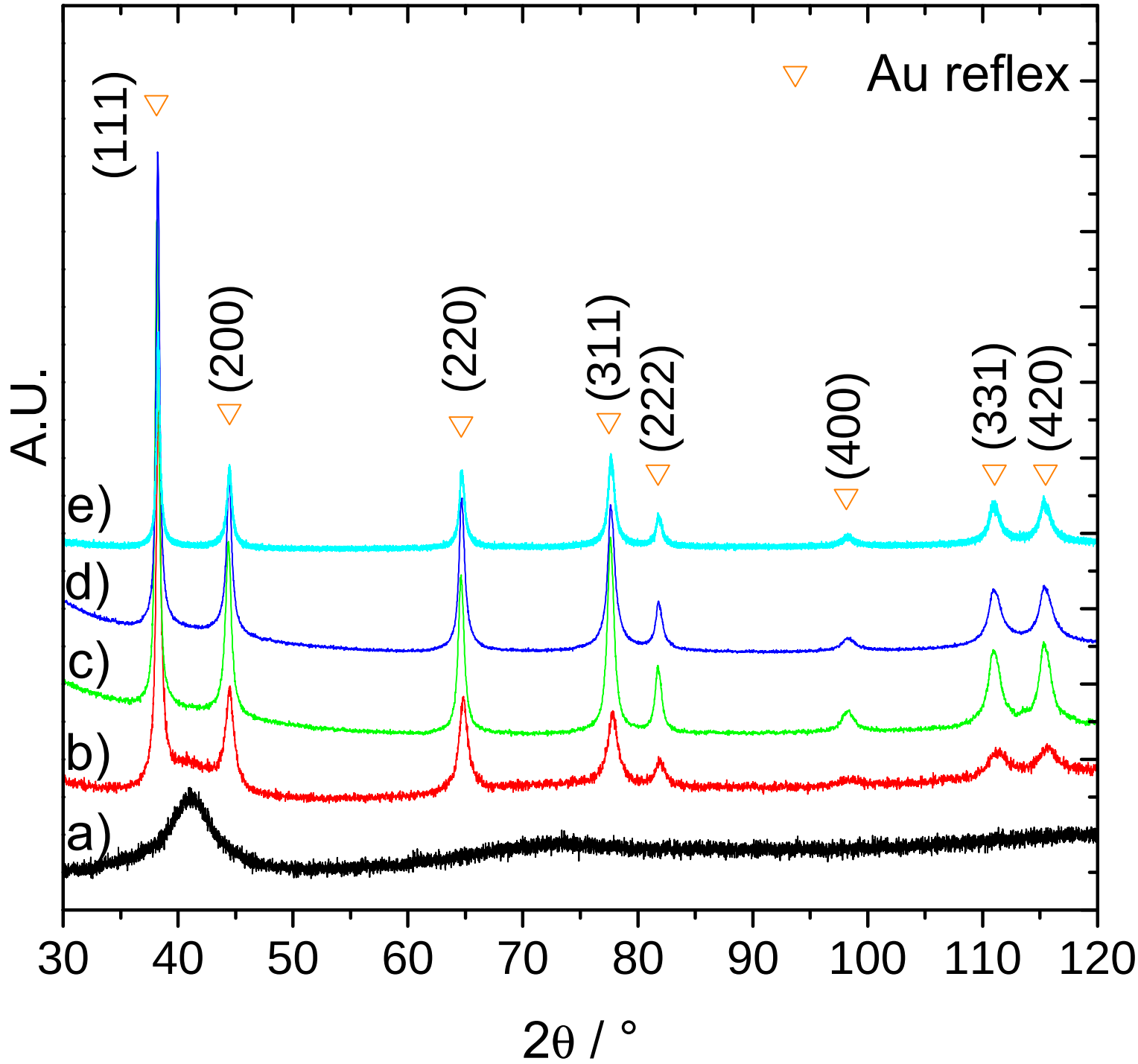
Au reflex
(111)
(200)
(220)
(311)
(222)
(400)
(331)
(420)
A.U.
e)
d)
c)
b)
a)
30
40
50
60
70
80
90
100
110
120
2θ / °

Figure

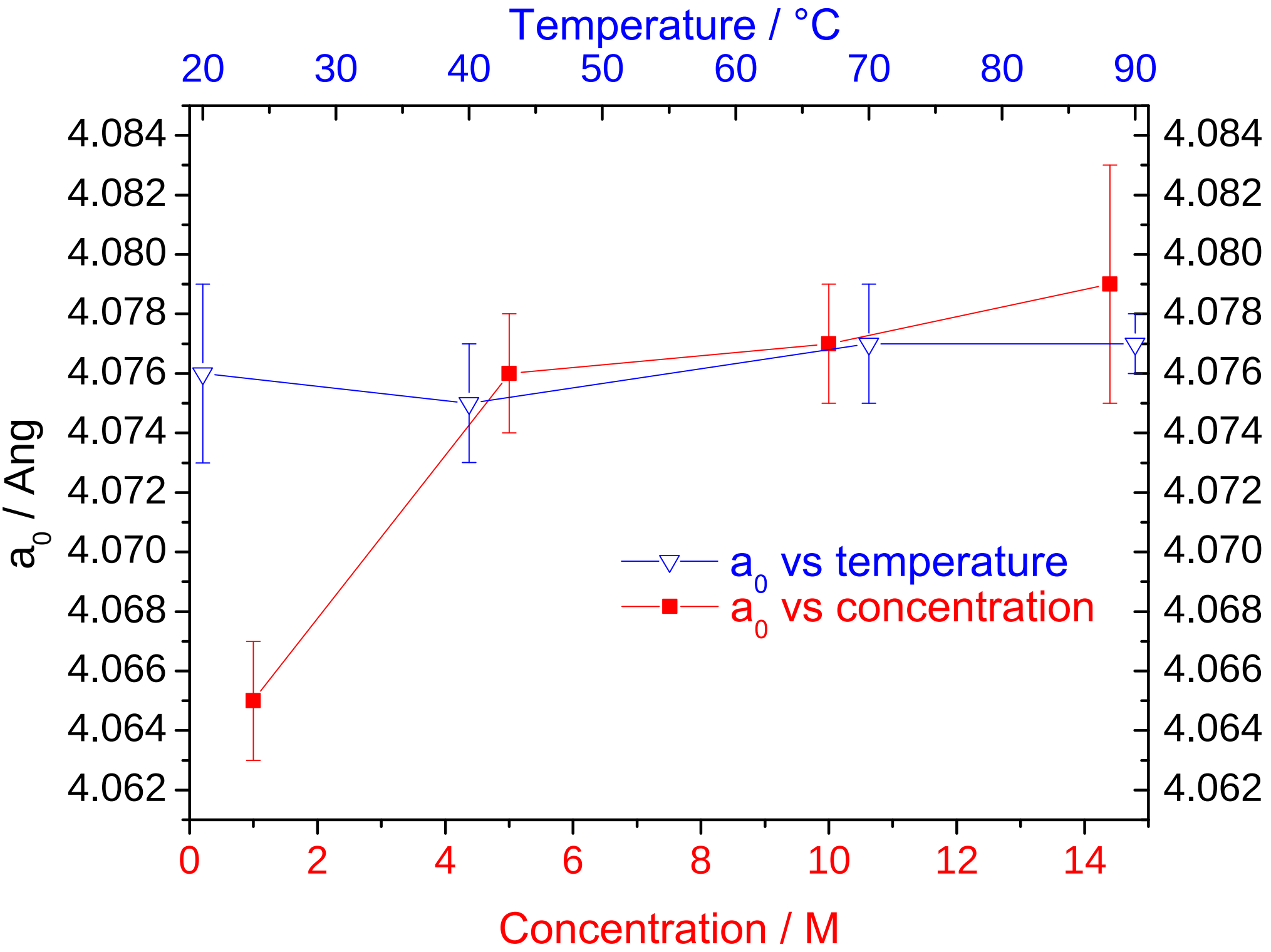
Temperature / °C
20
30
40
50
60
70
80
90
4.084
4.082
4.080
4.078
4.076
4.074
4.072
4.070
4.068
4.066
4.064
4.062
a0 / Ang
a0 vs temperature
a0 vs concentration
0
2
4
6
8
10
12
14
Concentration / M

Figure

Click here to download high resolution image

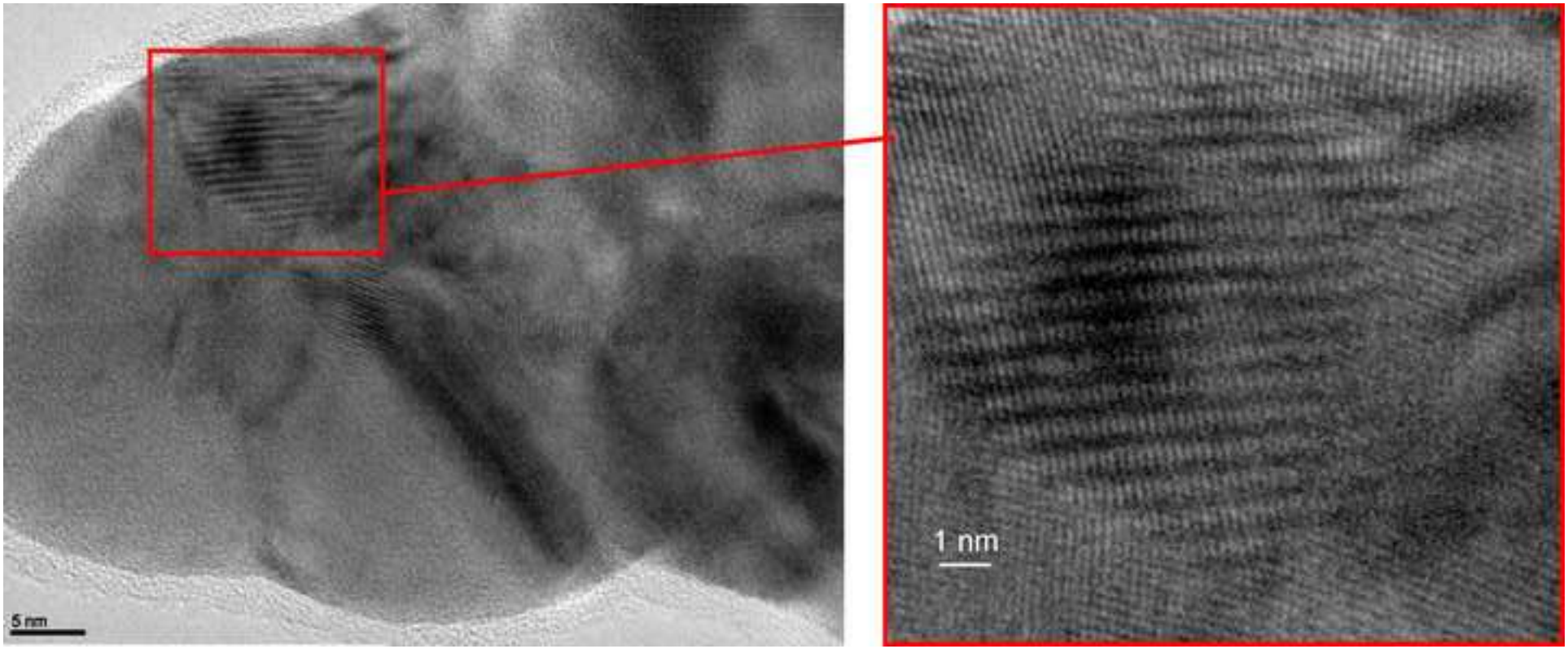

Figure

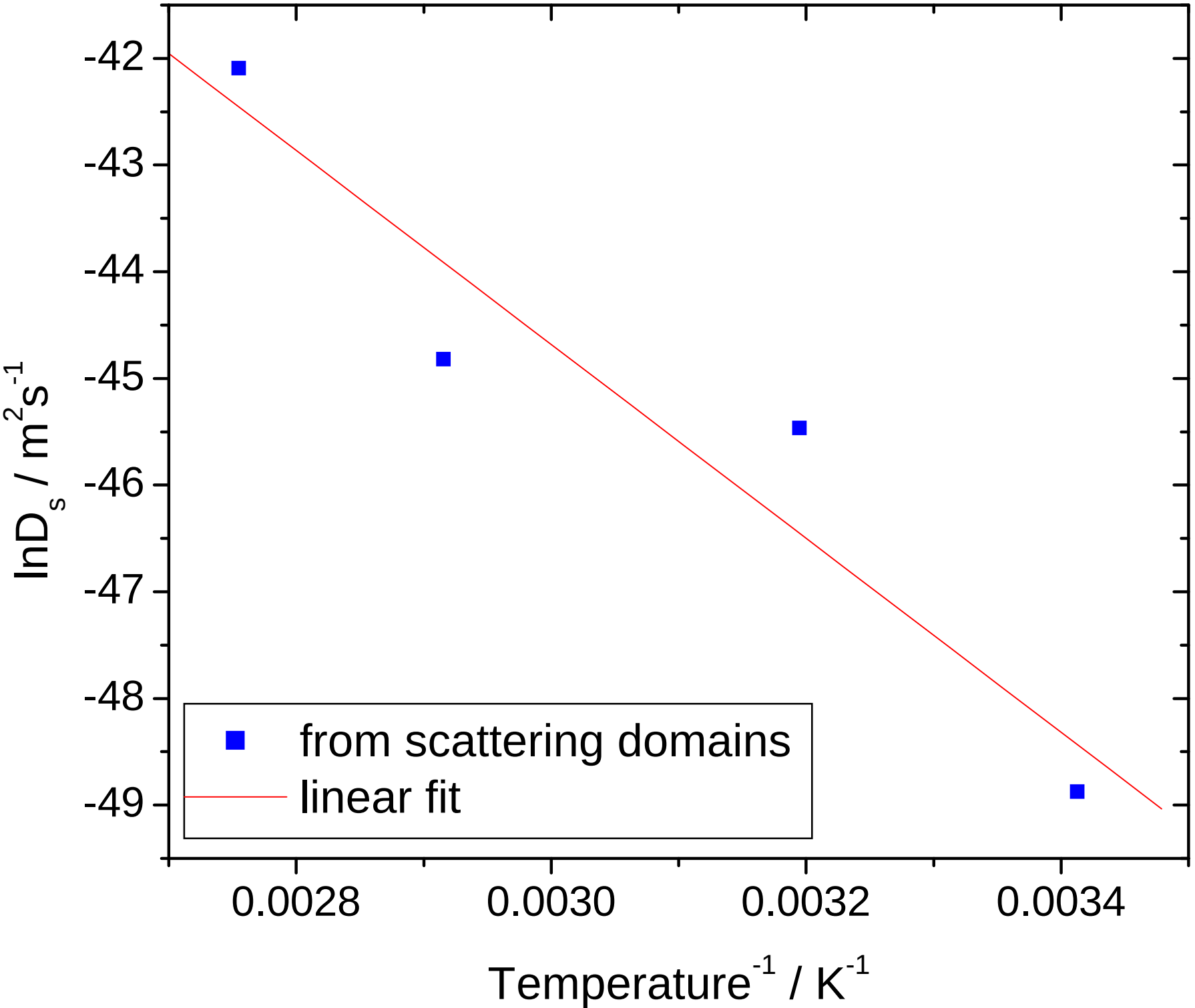
-42
-43
-44
-45
-46
-47
-48
-49
lnD_s / m^2s^-1
0.0028
0.0030
0.0032
0.0034
Temperature^-1 / K^-1
from scattering domains
linear fit

Supplementary Material for on-line publication only

Click here to download Supplementary Material for on-line publication only: Supporting information.docx